Int J Adv Manuf Technol (2006) 30: 118–128
DOI 10.1007/s00170-005-0047-4

ORIGINAL ARTICLE

Yanchun Xia · Yuehong Yin · Zhaoneng Chen

Dynamic analysis for peg-in-hole assembly with contact deformation

Received: 20 October 2004 / Accepted: 16 March 2005 / Published online: 1 December 2005

Abstract The dynamic model is established based on compliance contact mechanics in this paper. The relationship is obtained between parameters, such as input force/torque, reaction contact forces/moment, contact pressure, contact deformation, etc. The traditional rigid body dynamic model with friction contact is limited. Inconsistencies and ambiguities can arise in such a model and the frictional impact can lead to violating principles of energy conservation. However, in light of physical characteristic of the system, the compliant contact dynamic model of this system can overcome these problems. Jamming and wedging are two ill-poses in assembly operation. On the basis of the dynamic model, the no-jamming and no-wedging assembly strategies can be obtained.

Keywords Assembly · Contact deformation · Dynamic analysis · Jamming · Wedging

1 Introduction

Robot assembly is a constraint manipulation. Due to the uncertainties of an exterior environment, such as the orientation of accessories, robot movement and sensor information in the process of actual robotic actual assembly, abrupt incidents etc., assembly part often deviates from ideal trace and leads to contact and collision with the environment. In traditional position control, the small relative positional misalignments, which inevitably occur in assembly operations of this type, will lead to excessively large contact forces, which can lead to invalidation, destroy the assembly parts or circumjacent fixtures and even engender assembly operation to failure at last. So, whether the assembly operation succeeds or fails is closely related with mating strategies and contact mechanics. Robot assembly operation is virtually force-guided parts mating motion process. It includes the establishment of physical contact relations between parts (geometric constraints) and compliant motion under force constraints. However, constraint forces can be obtained by special contact states. So it is very important for robot assembly analysis to understand the issue of contact mechanics. The analysis of contact mechanics has a profound bearing on the ability of a robotic system to recognize sensory errors and reduce geometric and control uncertainties and invoke corrective assembly actions.

An assembly part is subject to multiple frictional contacts with other objects in assembly operation. In most previous works, a part can be regarded as a rigid object. Under such assumption, there are two basic problems that cannot be easily solved [1]. One is inconsistencies and ambiguities of solution to rigid dynamic model with the coulomb's friction law. The other is violating principles of energy conservation under traditional frictional impact model. The compliant elastic contact model can accurately analyze the dynamic assembly operation. The relationship is obtained between parameters, such as input force/torque, reaction contact forces/moment, contact pressure, contact deformation, etc. in the model. The analysis of contact mechanics involves impact dynamics, sliding dynamics, the contact conditions, frictional law as well as the analysis of stability. For many years, many scholars have applied the theory of classical contact mechanics to robot operations. Wang and Mason [2] have modeled the impact dynamics of robotic operations. Rajan [3] et al. have discussed the sliding dynamics for rigid bodies in contact with frictional surfaces. Pramath [4] et al. analyzed the contact stress for multiple grasping model. The constraints that arise in contact bodies are called unilateral constraints, because the contact forces and relative displacements can be defined so that they are non-negative. Mei [5] et al. defined and explained the unilateral constraints. Pierre [6] et al.

Y. Xia (✉) · Y. Yin · Z. Chen
Research Institute of Robotics,
Shanghai Jiao Tong University,
1954 Huashan Road,
200030 Shanghai, People's Republic of China
e-mail: xiayanchun@sjtu.edu.cn
Tel.: +021-62933037

modeled the contacts using springs and dampers. A singular perturbation analysis is performed to ensure contact force stability in his model.

In the assembly process, jamming and wedging are two ill-poses which can lead to undesirable high strains on the parts or even the unfeasibility of the assembly task. At present, many scholars have made great efforts on handling these problems from three main aspects. One aspect is the use and study of different control strategies for the insertion. Through sensor signals the contact state is detected. If the strategy is proper for insertion system, the undesired contact forces can be reduced to low or even to zero [7]. The second solution is developing special compliant mechanisms based on RCC [8], such as SRCC [9] and DRCC [10]. The third approach is theoretical investigation. Through more accurate modeling, many problems that arose in the assembly process were analyzed in order to understand the insertion mechanics and reduce the uncertainties. Seyfferth [11] et al. presented the dynamics of the complete parts mating process including a full dynamical model of the manipulator. Whitney [12] et al. analyzed the jamming and wedging conditions in quasi-static states. Villarreal [13] et al. considered the elasticity in the workpieces in order to simplify the task planning process. Meitinger [14] et al. showed the nonlinear and unsteady mating forces arising during the insertion.

In this paper we make efforts on theory investigation to analyze proper assembly strategies, by which jamming and wedging can be avoided in the assembly process. At first, under traditional Hertz contact theory, the compliant contact model is established. In the second section the elastic contact dynamical model of peg-in-hole is established based on geometric constraints and deformable information. It is more accurate than traditional rigid dynamic models. At last, the jamming and wedging was analyzed based on the dynamical model and the proper assembly strategies are taken.

2 Compliant contact model

Although rigid body models work very well for unconstrained mechanical systems, they are not adequate for modeling systems with unilateral, frictional constraints. For a unilateral constraint system, contact forces cause deformation. It is necessary to adopt a compliant contact model that incorporates force/deformation relations for the master object and slave object. The main benefit of this approach is that it allows small deformations at each contact and because of this, the problem of static indeterminacy is automatically resolved. It is assumed that the deformations are small and the pressure is distributed over an area that is small compared to the dimensions of the object and deformable objects obey the laws of linear elasticity. The distance norm to the surface, which can be moved after making contact, and shapes of the elastic contact deformable zones are the main deformable analysis criterions. The elastic contact deformable zones in the assembly process will depend on several factors, namely the Young's modulus of workpiece material and the maximum allowable contact force, the orientation of the workpiece and the contact point, the direction of movement and the shape of the contact surface. All these factors are influenced by features of the workpiece and environment or strategies of planning and control. In order to keep the deformation within the limitation of elastic deformation that cannot destroy the assembly parts, it is important to avoid or reduce influences of exoteric factors.

2.1 Unilateral contact law

Let the profiles of the two contacting bodies be given by z_1 and z_2. Assume u_{n1} and u_{n2} are the deformations for contact zones. If δ_n denotes the relative rigid body displacement in the normal direction at the contact point. Then we can get

$$g = z_1 + z_2 + u_{n1} + u_{n2} - \delta_n. \tag{1}$$

To avoid penetration of the bodies into each other, the normal contact distance defined in Eq. 1 has to be greater than or equal to zero, i.e., g≥0. Contact between two bodies is now locally characterized by a unilateral contact condition, a compression condition and a complementary condition as follows:

$$g \geq 0,\ f_n \geq 0 f_n\, g = 0. \tag{2}$$

The unilateral contact condition requires that the master contact body and the slave contact body cannot penetrate each other. The compression condition shows that the two contact bodies cannot pull each other. Finally, the complementary condition indicates that the slave contact body is either separated from the master contact body $(g > 0, f_n = 0)$ or it presses on it $(g = 0, f_n \geq 0)$. These conditions are shown in Fig. 1.

2.2 Friction law

Coulomb's classical friction law is considered in this paper. In this law, it is assumed that two bodies in steady contact

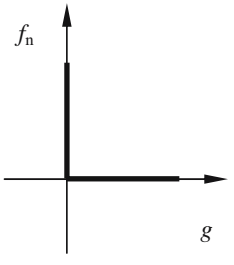

Fig. 1 Unilateral contact

either stick to each other or they slip on each other, depending on the following conditions:

$$g > 0, \Rightarrow f_n = 0, f_t = 0 \text{ (no contact)} \tag{3}$$

$$g = 0, |f_t| < \mu_s |f_n| \Rightarrow f_n \geq 0, u_t^1 - u_t^2 = 0 \text{ (Stick condition)} \tag{4}$$

$$g = 0, |f_t| = \mu_k |f_n| \Rightarrow f_n \geq 0, |u_t^1 - u_t^2| \geq 0 \text{(Slip condition)} \tag{5}$$

where μ_s and μ_k are the static and slipping coefficient of friction respectively, and $\mu_s \geq \mu_k$. u_t^1 and u_t^2 are tangential displacement of the body 1 and the body 2.

At the contact point, the reaction contact force $\boldsymbol{f}$ is the vector resultant of the normal contact force $\boldsymbol{f_n}$ and the tangential contact force $\boldsymbol{f_t}$, i.e., $\boldsymbol{f}=\boldsymbol{f_n}+\boldsymbol{f_t}$. Stick and slip states are depicted through relations of motion velocity v and tangential contact force f_t in Fig. 2. When slipping, $f_t=\mu_k f_n$, and when stick, $f_t=\mu_s f_n$. Reaction contact forces are influenced by applied forces and motion forms. However, all of reaction forces fall into a friction cone defined by $\alpha=tg^{-1}(\mu_s)$, as shown in Fig. 3. If the inertial force lies inside friction cone, the contact bodies cannot move. Similarly, if the body starts from rest then motion will ensure only if the inertial force lies outside the friction cone. When the inertial force on the friction cone boundary, it is a critical motion state.

2.3 Contact analysis

It is assumed that the shape of deformation zones is ellipse under contact forces. According to classical Hertz theories, the profiles of the two contacting bodies can be given by the following forms:

$$z_i = \frac{1}{2\rho_{i1}}x^2 + \frac{1}{2\rho_{i2}}y^2 \tag{6}$$

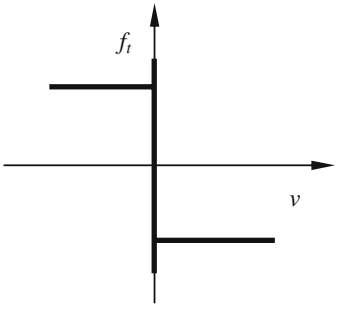

Fig. 2 Frictional contact force

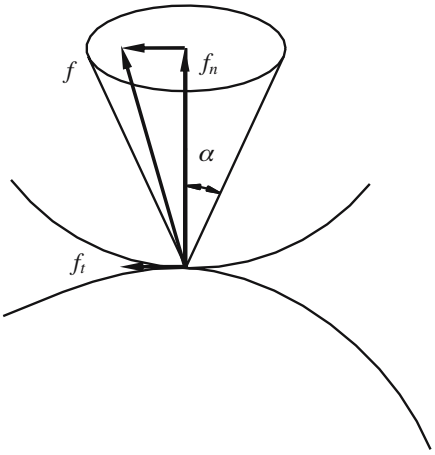

Fig. 3 Frictional cone

where ρ_{i1} and ρ_{i2} are the main curvature radius, and the sum of them is

$$\sum \rho = \sum_{i=1,2;j=1,2} \rho_{ij}. \tag{7}$$

The ellipse contact deformation zone can be expressed:

$$\frac{x^2}{a^2} + \frac{y^2}{b^2} = 1 \tag{8}$$

$$a = m_a \sqrt[3]{\frac{3Q}{2\sum \rho}\left(\frac{1-\nu_1^2}{E_1} + \frac{1-\nu_1^2}{E_1}\right)} \tag{9}$$

$$b = m_b \sqrt[3]{\frac{3Q}{2\sum \rho}\left(\frac{1-\nu_1^2}{E_1} + \frac{1-\nu_1^2}{E_1}\right)}. \tag{10}$$

The maximum contact pressure is

$$p_0 = \frac{3}{2}\frac{Q}{\pi ab} \quad . \tag{11}$$

The contact deformation is

$$u = \frac{1-\nu^2}{E} b p_0 \left[A - B\frac{x^2}{a^2} - C\frac{y^2}{b^2}\right] \quad . \tag{12}$$

The maximum contact deformation, i.e., the relative rigid body displacement in the normal direction at the contact point can be obtained

$$\delta_n = K \sqrt[3]{\frac{1}{8}\left[\frac{3}{2}\left(\frac{1-\nu_1^2}{E_1} + \frac{1-\nu_2^2}{E_2}\right)\right]^2 Q^2 \sum \rho}, \tag{13}$$

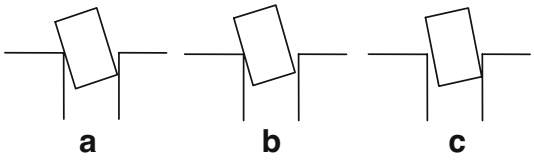

Fig. 4 Contact states peg–in–hol

where m_a, m_b, A, B, C and K are the deformable influence coefficients. E is the Young's modulus of material, ν is the Poisson ratio, and Q is the contact force.

From above analysis, formula functions Eqs. 8, 9, 10, 11, 12, 13 expound the relations of deformable zone, contact pressure, contact forces, deformations, and the relative displacement. The contact forces can be expressed by applied forces, and the maximum contact force is restricted by the material yield-limited expressed by the inequality $Q \leq Q_{max}$. Also, the applied forces are restricted by the maximum carrying capacity of the robot's end-effector. So, the limit carrying capacity of the system can be obtained.

3 Dynamics of pet into deformable hole

The dynamical model of peg into deformable hole is established in this section. In the insertion process, there exist position errors and orientation errors. If the peg is inserted with one side alignment, positive or negative, there are three possible states when peg-in-hole [12], as shown in Fig. 4. If consider all situations, there are six possible states. Here we consider the two point contact state shown in Fig. 4a and establish the rectangular Cartesian coordinate system XY, shown in the Fig. 5.

As is shown in Fig. 5, it is reasonably assumed that the deformed area of each contact point is ellipse-shaped as black-painted in the figure and the position variables of the center of mass C of the peg and manipulator is expressed as $P_c(x,y,\theta)$. At different contact point, let the maximum deformations be $\delta_i,(i = A, B)$. A(x_{Ac},y_{Ac}) and B(x_{Bc},y_{Bc}) are the deformation contact points. The relations between them can be expressed as:

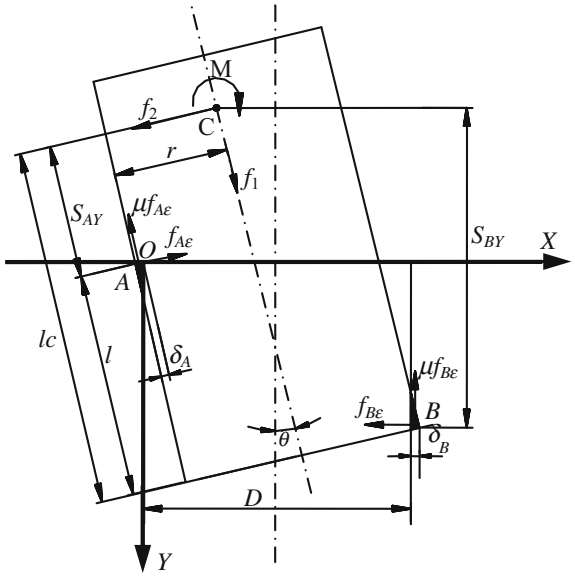

Fig. 5 Two–point contact state

$$\delta_A = -x_{Ac}\cos\theta + y_{Ac}\sin\theta \tag{14}$$

$$\delta_B = x_{Bc} - D. \tag{15}$$

Let $f_{A\varepsilon}$ and $f_{B\varepsilon}$ be the contact forces whose directions are perpendicular to the surface of the object as shown by arrows in Fig. 5, and the magnitude of the forces pressing the object are expressed as a function of δ_{in}. Then the frictional forces $\mu f_{A\varepsilon}$ and $\mu f_{B\varepsilon}$ can be obtained.

3.1 Geometrical constraints

Constraint forces are arose from geometric constraints and applied forces. However, the geometrical constraints can be shown in the following:

$$\begin{aligned} x &= x_{Ac} + S_{AX}\cos\theta - S_{AY}\sin\theta \\ &= x_{Bc} - S_{BX} \end{aligned} \tag{16}$$

$$\begin{aligned} y &= y_{Ac} - S_{AX}\sin\theta - S_{AY}\cos\theta \\ &= y_{Bc} - S_{BY}, \end{aligned} \tag{17}$$

where

$$x_{Ac} = -\delta_A\cos\theta \tag{18}$$

$$y_{Ac} = \delta_A\sin\theta \tag{19}$$

$$x_{Bc} = D + \delta_B \tag{20}$$

$$y_{Bc} = l\cos\theta - (d - \delta_A)\sin\theta \tag{21}$$

$$S_{AX} = r \tag{22}$$

$$S_{AY} = l_c - l \tag{23}$$

$$\begin{aligned} l &= \left[S_{BY}^2 + D_B^2 - d_A^2\right]^{1/2} \\ &= \frac{D + \delta_A\cos\theta + \delta_B - d\cos\theta}{\sin\theta} \end{aligned} \tag{24}$$

$$D_B = D + \delta_B \quad d_A = d - \delta_A$$

$$S_{BX} = l_c \sin\theta + r\cos\theta. \tag{25}$$

$$S_{BY} = l_c \cos\theta - r\sin\theta. \tag{26}$$

S_{AX} and S_{AY} are distances of point A to C at the norm direction and the tangential direction, respectively. Similarly, S_{BX} and S_{BY} are norm and tangential distances of point B to C. l_c is the distance form C to the bottom line of the peg. l is the insertion depth and θ is the title angle between peg and hole.

Unite Eqs. 16, 17, 18, 19, 20, 21, 22, 23, 24, 25, 26, we can get

$$\begin{aligned} x &= x_{Ac} + S_{AX}\cos\theta - S_{AY}\sin\theta \\ &= -\delta_A\cos\theta + r\cos\theta - (l_c - l)\sin\theta \end{aligned} \tag{27}$$

$$\begin{aligned} y &= y_{Ac} - S_{AX}\sin\theta - S_{AY}\cos\theta \\ &= \delta_A\sin\theta - r\sin\theta - (l_c - l)\cos\theta \end{aligned} \tag{28}$$

or

$$\begin{aligned} x &= x_{Bc} - S_{BX} \\ &= D + \delta_B - l_c\sin\theta - r\cos\theta \end{aligned} \tag{29}$$

$$y = y_{Bc} - S_{BY} = -(l_c - l)\cos\theta - (r - \delta_A)\sin\theta. \tag{30}$$

3.2 The dynamic of constraints

Consider an n degree of freedom system with generalized coordinates given by the vector p which is subject to the m unilateral constraints, we can get the constrained dynamic equation using Lagrange multipliers.

$$M(p)\ddot{p} + f_\mu + g_{\varepsilon p}^T(p,t)\lambda = U \tag{31}$$

$$U = q_p u$$

where, $M(p)$=dig(m,m,J)denotes the diagonal matrix whose diagonal matrices stand for the mass of the object and the inertial moment at the mass center C in the Cartesian coordinates XY. u is n×1 vector function which includes external forces and torques. q_p denotes the n×n Jacobian matrix of the input forces and torques with respect to the coordinate space XY. λ is the m×1 rector of multipliers or constraint forces, which is virtually caused by contact deformable forces mentioned above. f_μ is the m×1 vector of frictional forces, and $g_{\varepsilon p}^T(p,t)$ is a n×m Jacobian matrix whose columns represent the directions of the m unilateral constraints.

Following the Coulomb model, we assume friction force at the contact point to depend linearly on the contact forces. If frictional coefficients μ_i are the same in the system, we can get

$$f_\mu = \mu\hat{g}_{\varepsilon p}^T(p,t)\lambda = -\mu\,\mathrm{sgn}(v_{ct})\lambda \tag{32}$$

where v_{ct} is the tangential velocity at contact point.

Substituting Eq. 32 to Eq. 31, we obtain

$$\begin{aligned} &M(p)\ddot{p} + [g_{\varepsilon p}^T(p,t) + \mu\hat{g}_{\varepsilon p}^T(p,t)]\lambda = U \\ &M(p)\ddot{p} + G_p^T(p,t)\lambda = U \end{aligned} \tag{33}$$

where

$$\lambda = \begin{pmatrix} \lambda_1 \\ \lambda_2 \end{pmatrix} = \begin{pmatrix} f_{A\,\varepsilon} \\ f_{B\,\varepsilon} \end{pmatrix} \tag{34}$$

$$g_{\varepsilon p}^T(p,t) = [g_{\varepsilon A}^T(p,t)\; g_{\varepsilon B}^T(p,t)] \tag{35}$$

$$\hat{g}_{\varepsilon p}^T(p,t) = [\hat{g}_{\varepsilon A}^T(p,t)\; \hat{g}_{\varepsilon B}^T(p,t)]. \tag{36}$$

The different part of the dynamics can be formulated in the following ways. At first, the first and second derivative can be obtained by Eqs. 29 and 30, so we have $\ddot{p}$

$$\dot{x} = K_{x1}\cos\theta + K_{x2}\sin\theta \tag{37}$$

$$\begin{aligned} \dot{y} &= K_{y1}\sin\theta + K_{y2}\cos\theta, \text{ where } K_{x1} = -l_c\dot{\theta},\ K_{x2} \\ &= r\dot{\theta},\ K_{y1} = (l_c - l)\dot{\theta},\ K_{y2} = \dot{l} - (r - \delta_A)\dot{\theta} \end{aligned} \tag{38}$$

$$\ddot{x} = K_{x3}\sin\theta + K_{x4}\cos\theta \tag{39}$$

$$\ddot{y} = K_{y3}\sin\theta + K_{y4}\cos\theta \tag{40}$$

where

$$\begin{aligned} K_{x3} &= l_c\dot{\theta}^2 + r\ddot{\theta}, \\ K_{x4} &= r\dot{\theta}^2 - l_c\ddot{\theta}, \\ K_{y3} &= (r - \delta_A)\dot{\theta}^2 - 2\dot{l}\dot{\theta} + (l_c - l)\ddot{\theta} \\ K_{y4} &= (l_c - l)\dot{\theta}^2 + \ddot{l} - (r - \delta_A)\ddot{\theta}. \end{aligned}$$

According to Eqs. 24 and 26

$$\dot{l} = S_{BY}\dot{S}_{BY}\Big/ l \quad \& \quad \dot{S}_{BY} = -l_c\dot{\theta}\sin\theta - r\dot{\theta}\cos\theta \tag{41}$$

or

$$\dot{S}_{BY} = \dot{l}l\Big/ S_{BY} \,\&\, \dot{\theta} = -\frac{\dot{S}_{BY}}{l_c\sin\theta + r\cos\theta} \tag{42}$$

$$\begin{aligned}\ddot{l} &= \frac{\dot{S}_{BY}^2 + S_{BY}\ddot{S}_{BY}}{l} - \frac{\dot{l}S_{BY}\dot{S}_{BY}}{l^2} \quad \& \\ \ddot{S}_{BY} &= \left(r\dot{\theta}^2 - l_c\ddot{\theta}\right)\sin\theta - \left(l_c\dot{\theta}^2 + r\ddot{\theta}\right)\cos\theta\end{aligned} \tag{43}$$

or it can be expressed in another way.

$$\begin{aligned}\ddot{S}_{BY} &= \frac{\dot{l}^2 + l\ddot{l} - \dot{S}_{BY}^2}{S_{BY}} \& \\ \ddot{\theta} &= \frac{(r\sin\theta - l_c\cos\theta)\dot{\theta}^2 - \ddot{S}_{BY}}{l_c\sin\theta + r\cos\theta}\end{aligned} \tag{44}$$

For constraints Jacobian matrix, we have

$$\begin{aligned}g_{\varepsilon A}^T(p,t) &= \left(\frac{\partial\delta_A}{\partial x}, \quad \frac{\partial\delta_A}{\partial y}, \quad \frac{\partial\delta_A}{\partial\theta}\right)^T \\ &= \begin{bmatrix}\frac{\partial x_{Ac}}{\partial x} & \frac{\partial x_{Ac}}{\partial y} & \frac{\partial x_{Ac}}{\partial\theta} \\ \frac{\partial y_{Ac}}{\partial x} & \frac{\partial y_{Ac}}{\partial y} & \frac{\partial y_{Ac}}{\partial\theta}\end{bmatrix}^T \begin{pmatrix}\frac{\partial\delta_A}{\partial x_{Ac}} \\ \frac{\partial\delta_A}{\partial y_{Ac}}\end{pmatrix} \\ &= \begin{bmatrix}1 & 0 & S_{AX}\sin\theta + S_{AY}\cos\theta + \dot{S}_{AY}\sin\theta \\ 0 & 1 & S_{AX}\cos\theta - S_{AY}\sin\theta + \dot{S}_{AY}\cos\theta\end{bmatrix}^T \\ &\quad \times \begin{pmatrix}-\cos\theta \\ \sin\theta\end{pmatrix} = \begin{bmatrix}-\cos\theta & \sin\theta & -S_{AY}\end{bmatrix}^T\end{aligned} \tag{45}$$

$$\begin{aligned}g_{\varepsilon B}^T(p,t) &= \left(\frac{\partial\delta_B}{\partial x}, \quad \frac{\partial\delta_B}{\partial y}, \quad \frac{\partial\delta_B}{\partial\theta}\right)^T \\ &= \begin{bmatrix}\frac{\partial x_{Bc}}{\partial x} & \frac{\partial x_{Bc}}{\partial y} & \frac{\partial x_{Bc}}{\partial\theta} \\ \frac{\partial y_{Bc}}{\partial x} & \frac{\partial y_{Bc}}{\partial y} & \frac{\partial y_{Bc}}{\partial\theta}\end{bmatrix}^T \begin{pmatrix}\frac{\partial\delta_B}{\partial x_{Bc}} \\ \frac{\partial\delta_B}{\partial y_{Bc}}\end{pmatrix} \\ &= \begin{bmatrix}1 & 0 & l_c\cos\theta - r\sin\theta \\ 0 & 1 & -l_c\sin\theta - r\cos\theta\end{bmatrix}^T \begin{pmatrix}1 \\ 0\end{pmatrix} \\ &= \begin{bmatrix}1 & 0 & S_{BY}\end{bmatrix}^T\end{aligned} \tag{46}$$

$\hat{g}_{\varepsilon A}^T(p,t)$ and $\hat{g}_{\varepsilon B}^T(p,t)$ can be obtained at the same time.

$$\begin{aligned}\hat{g}_{\varepsilon A}^T(p,t) &= \left[\operatorname{sgn}(v_{cA})\sin\theta \quad \operatorname{sgn}(v_{cA})\cos\theta \quad \operatorname{sgn}(v_{cA})S_{AX}\right]^T \\ &= \left[\sin\theta \quad \cos\theta \quad S_{AX}\right]^T\end{aligned} \tag{47}$$

$$\begin{aligned}\hat{g}_{\varepsilon B}^T(p,t) &= \left[0 \quad sgn(v_{cB}) \quad -sgn(v_{cB})S_{BX}\right]^T \\ &= \left[0 \quad 1 \quad -S_{BX}\right]^T\end{aligned} \tag{48}$$

So,

$$\begin{aligned}G_p^T(p,t) &= g_{\varepsilon p}^T(p,t) + \mu\hat{g}_{\varepsilon p}^T(p,t) \\ &= \begin{bmatrix}-\cos\theta & \sin\theta & -S_{AY} \\ 1 & 0 & S_{BY}\end{bmatrix}^T \\ &\quad + \mu\begin{bmatrix}\sin\theta & \cos\theta & S_{AX} \\ 0 & 1 & -S_{BX}\end{bmatrix}^T \\ &= \begin{bmatrix}-\cos\theta + \mu\sin\theta & \sin\theta + \mu\cos\theta & S_{AX} - S_{AY} \\ 1 & \mu & S_{BY} - S_{BX}\end{bmatrix}^T\end{aligned} \tag{49}$$

As a result, the final dynamic equation of the peg-in-hole is

$$\begin{aligned}&\begin{bmatrix}m & 0 & 0 \\ 0 & m & 0 \\ 0 & 0 & J\end{bmatrix}\begin{bmatrix}\ddot{x} \\ \ddot{z} \\ \ddot{\theta}\end{bmatrix} \\ &+ \begin{bmatrix}-\cos\theta + \mu\sin\theta & \sin\theta + \mu\cos\theta & \mu S_{AX} - S_{AZ} \\ 1 & \mu & S_{BZ} - \mu S_{BX}\end{bmatrix}^T \\ &\times \begin{bmatrix}f_{A\varepsilon} \\ f_{B\varepsilon}\end{bmatrix} = \begin{bmatrix}\sin\theta & \cos\theta & 0 \\ \cos\theta & -\sin\theta & 0 \\ 0 & 0 & 1\end{bmatrix}\begin{bmatrix}f_1 \\ f_2 \\ M\end{bmatrix}\end{aligned} \tag{50}$$

where f_1, f_2 are components of the input force $\boldsymbol{F}$ in the axis and radial directions of the peg, respectively. M is the input torque.

According to the Eq. 50 and applying the D'Alember principle, yields

$$\begin{aligned}m\ddot{x} &= f_1\sin\theta + f_2\cos\theta + k_1 f_{A\varepsilon} - f_{B\varepsilon} \\ m\ddot{z} &= f_1\cos\theta - f_2\sin\theta - k_2 f_{A\varepsilon} - \mu f_{B\varepsilon} \\ J\ddot{\theta} &= M + (S_{AZ} - \mu S_{AX})f_{A\varepsilon} - (S_{BZ} - \mu S_{BX})f_{B\varepsilon}.\end{aligned} \tag{51}$$

So the contact forces and moments can be got using input forces and torques.

$$\begin{aligned}f_{A\varepsilon} &= a_1 f_1 + a_2 f_2 + a_3 \\ f_{B\varepsilon} &= b_1 f_1 + b_2 f_2 + b_3 \\ M &= c_1 f_1 + c_2 f_2 + c_3 + J\ddot{\theta}\end{aligned} \tag{52}$$

where,

$$
\begin{aligned}
a_1 &= k_1/k_3 \\
a_2 &= -k_2/k_3 \\
a_3 &= \left(\mu m\ddot{x} - m\ddot{z}\right)/k_3 \\
b_1 &= 1/k_3 \\
b_2 &= \mu/k_3 \\
b_3 &= -(k_1 m\ddot{z} + k_2 m\ddot{x})/k_3 \\
c_1 &= a_1(\mu S_{AX} - S_{AZ}) + b_1(S_{BZ} - \mu S_{BX}) \\
c_2 &= a_2(\mu S_{AX} - S_{AZ}) + b_2(S_{BZ} - \mu S_{BX}) \\
c_3 &= a_3(\mu S_{AX} - S_{AZ}) + b_3(S_{BZ} - \mu S_{BX}) \\
k_1 &= \cos\theta - \mu \sin\theta \\
k_2 &= \sin\theta + \mu \cos\theta \\
k_3 &= k_2 + \mu k_1 .
\end{aligned}
$$

When the contact state is one-point contact shown as Fig. 4b or c, then $f_{B\varepsilon} = 0$ or $f_{A\varepsilon} = 0$, and other contact force and moment can be obtained as the similar way, as follows:

$$
\begin{aligned}
m\ddot{x} &= -f_1 \sin\theta + f_2 \cos\theta - k_1 f_{A\varepsilon} \\
m\ddot{z} &= f_1 \cos\theta + f_2 \sin\theta - k_2 f_{A\varepsilon} \\
J\ddot{\theta} &= M + (S_{AZ} - \mu S_{AX}) f_{A\varepsilon}
\end{aligned}
\tag{53}
$$

$$
\begin{aligned}
m\ddot{x} &= f_1 \sin\theta + f_2 \cos\theta - f_{B\varepsilon} \\
m\ddot{z} &= f_1 \cos\theta - f_2 \sin\theta - \mu f_{B\varepsilon} \\
J\ddot{\theta} &= M - (S_{BZ} - \mu S_{BX}) f_{B\varepsilon}
\end{aligned}
\tag{54}
$$

Also, the contact forces and moments can be obtained using above the equations.

At the same argument, the establishment of dynamic equations and the solution of contact forces and moments of the system can be obtained when the peg is leaning the other way.

According to the analysis of the Sect. of 1.3 and the dynamical analysis, the maximum carrying capacity can be obtained and the range of input forces and torques can be further obtained. As a result, the input forces and torques can be properly set and adjusted under the condition that cannot destroy the workpiece and circumstance.

3.3 Energy analysis

It is now possible to show that the input–output pair (u, p) for the system of Eq. 31 satisfies passivity. In fact, in the light of physical meanings of Jacobian matrices in Eqs. 45, 46, 47, 48 and inner product between input and output is described as

$$
\begin{aligned}
\dot{p}^T U = &\frac{d}{dt}\left\{\frac{1}{2}\left(m\dot{x}^2 + m\dot{y}^2 + J\dot{\theta}^2\right)\right\} \\
&+ \left(\dot{x}_{Ac}, \dot{y}_{Ac}\right) f_{A\varepsilon} \begin{pmatrix} -\cos\theta \\ \sin\theta \end{pmatrix} + \left(\dot{x}_{Bc}, \dot{y}_{Bc}\right) f_{B\varepsilon} \begin{pmatrix} 1 \\ 0 \end{pmatrix} + f_\mu
\end{aligned}
\tag{55}
$$

From the geometric constraint Eqs. 14, 15, and 18, 19, 20, 21, we have

$$
\dot{\delta}_A = -\dot{x}_{Ac} \cos\theta + \dot{y}_{Ac} \sin\theta \tag{56}
$$

$$
\dot{\delta}_B = \dot{x}_{Bc}. \tag{57}
$$

So

$$
\dot{p}^T U = \frac{d}{dt}\left\{\frac{1}{2}\left(m\dot{x}^2 + m\dot{y}^2 + J\dot{\theta}^2\right)\right\} + \dot{\delta}_A f_{A\varepsilon} + \dot{\delta}_B f_{B\varepsilon} + f_\mu \tag{58}
$$

where

$$
K = \frac{1}{2}\left(m\dot{x}^2 + m\dot{y}^2 + J\dot{\theta}^2\right). \tag{59}
$$

Note that $f_{i\varepsilon} \geq 0$, and it is strictly increasing with increasing deformation δ_i, and

$$
\dot{\delta}_i f_{i\varepsilon} = \frac{d}{dt}\int_0^{\delta_i} f_{i\varepsilon}(\xi) d\xi \geq 0. \tag{60}
$$

Since the integral of the above equation for $\delta_i \geq 0$, and the frictional force can be ignored, then we have

$$
\int_0^t \dot{p}^T U = E(t) - E(0) \geq \quad -E(0) \tag{61}
$$

which shows the passivity, where

$$
E = K + \sum_{i=A,B} \int_0^{\delta_i} f_{i\varepsilon}(\xi) d\xi. \tag{62}
$$

So, we can get

$$
P = \sum_{i=A,B} \int_0^{\delta_i} f_{i\varepsilon}(\xi) d\xi. \tag{63}
$$

If the frictional force is considered, the system energy is

$$E = K + P - S_\mu. \tag{64}$$

4 Strategies for dynamic assembly

The assembly process is virtually the dynamical adjustment under geometrical constraints and force constraints. If these constraints are not proper, the ill-pose situations can arise, such as jamming and wedging.

4.1 Jamming analysis

Jamming is a condition in which the peg will not move because the forces and moments applied to the peg through the support are in the wrong proportions. In fact, it is a state that the inertia force is collinear with the reaction force. There are two situations. One is that the inertia force is collinear with the reaction force inside the friction cone, which cannot make the system move; the other is that the inertia force is collinear with the reaction force on the edge of the friction cone. In the onset of the second jamming situation, despite finite input forces and torques, the relevant contact and friction forces, as well as acceleration, approach infinity producing loss of a degree of freedom under impact-like conditions.

According to the above dynamical analysis result, and the jamming definition, the no-jamming conditions, and space can be analyzed in the following section.

4.1.1 Two dimension jamming analysis

When the contact state is one-point contact shown as Fig. 4b or c, there exists two degree of freedom. The peg can translate and rotate along the axis of the hole. Here, we only consider occurring translations or rotations, but not simultaneously.

In Fig. 4c, the peg contacts the wall of the hole at point B. If the direction of the inertial force is outside the friction cone, i.e., the angle between the inertial force vector and normal contact vector is greater than the friction cone angle at this constraint point, it satisfied no-jamming conditions. So the following inequality has to be satisfied:

$$\frac{m\ddot{z}}{m\ddot{x}} = \frac{f_1\cos\theta - f_2\sin\theta - \mu f_{B\varepsilon}}{f_1\sin\theta + f_2\cos\theta - f_{B\varepsilon}} > \mu \tag{65}$$

so,

$$\frac{f_2}{f_1} < \frac{\cos\theta - \mu\sin\theta}{\sin\theta + \mu\cos\theta}. \tag{66}$$

Also, according to Eqs. 51, 52, 53, 54, we can get

$$\frac{M}{rf_1} = k_{b1}\frac{f_2}{f_1} + b_{b1} + \frac{c_{b1} + J\ddot{\theta}}{rf_1} \tag{67}$$

where, $k_{b1} = \frac{(S_{BZ} - \mu S_{BX})\cos\theta}{r}$

$b_{b1} = \frac{(S_{BZ} - \mu S_{BX})\sin\theta}{r}$

$c_{b1} = -(S_{BZ} - \mu S_{BX})m\ddot{x}$.

It is assumed that $J\ddot{\theta} = 0$, the above equation can be transformed into followed inequality.

$$\frac{M}{rf_1} \le k_{b1}\frac{f_2}{f_1} + b_{b1}. \tag{68}$$

Considering the opposite state of Fig. 4c, we have:

$$\frac{f_2}{f_1} > \frac{\mu\sin\theta - \cos\theta}{\sin\theta + \mu\cos\theta} \tag{69}$$

$$\frac{M}{rf_1} \ge k_{b2}\frac{f_2}{f_1} + b_{b2} \tag{70}$$

where $k_{b2} = k_{b1} = k_b$

$b_{b2} = -b_{b1} = -b_b$.

So,

$$\left|\frac{f_2}{f_1}\right| < \frac{\cos\theta - \mu\sin\theta}{\sin\theta + \mu\cos\theta} \tag{71}$$

$$\left|\frac{M}{rf_1}\right| \le k_b\frac{f_2}{f_1} \pm b_b. \tag{72}$$

For Fig. 4b, according to the above analysis, we have

$$\left|\frac{f_2}{f_1}\right| < \frac{1}{\mu} \tag{73}$$

$$\left|\frac{M}{rf_1}\right| \le k_a\frac{f_2}{f_1} \tag{74}$$

where, $k_a = l_c - l - \mu r$. Because the insertion depth l is not sure at the one-point contact state, the value k_α is uncertainty.

So to avoid one-point jamming the inequalities Eqs. 71, 72, 73, 74 must be satisfied, especially Eqs. 71 and 73.

When the contact state is two-point contact state as shown in Fig. 4a, there are two contact constraints at points A and B. To avoid two-point jamming, the inertial force must be outside the friction cone and the inertial moment is propitious to adjusting the peg into the hole. On the basis of the above analysis of one-point contact states, the following inequalities have to be satisfied.

$$-\frac{1}{\mu} < \frac{f_2}{f_1} < \frac{\cos\theta - \mu\sin\theta}{\sin\theta + \mu\cos\theta} \tag{75}$$

$$\& \quad J\ddot{\theta} < 0. \tag{76}$$

Combining Eqs. 52 and 76, we have

$$\frac{M}{rf_1} < k_{ab}\frac{f_2}{f_1} + b_{ab} + c_{ab} \tag{77}$$

$$\text{where, } \begin{matrix} k_{ab} = \frac{c_2}{r} \\ b_{ab} = \frac{c_1}{r} \\ c_{ab} = \frac{c_3}{rf_1} \end{matrix} \text{ here, } c_{ab} \le 0, \text{ so,}$$

$$\frac{M}{rf_1} < k_{ab}\frac{f_2}{f_1} + b_{ab}. \tag{78}$$

For symmetrical two-point contact state that the peg leaned the other way, the no-jamming conditions can be easily obtained

$$\frac{\mu\sin\theta - \cos\theta}{\sin\theta + \mu\cos\theta} < \frac{f_2}{f_1} < \frac{1}{\mu} \tag{79}$$

$$\frac{M}{rf_1} > k_{ab}\frac{f_2}{f_1} - b_{ab}. \tag{80}$$

All of the above can be summarized in Fig. 6. The jamming diagrams are changeable with the insertion depth. At certain depth, the jamming diagram can be a parallelogram. On the parallelogram's edges, the peg can equilibrium slide in the hole. Outside the parallelogram, jamming can be occurred. Inside, the peg is in disequilibrium sliding or falling in.

4.1.2 Three dimension jamming analysis

In three dimensional space, we may represent the force to be applied to the peg in spherical coordinates as a magnitude $\boldsymbol{F}$ and two angles, $\boldsymbol{\beta}$ and $\boldsymbol{\gamma}$, *and* the applied moment as three orthogonal components ($\boldsymbol{M_x}$, $\boldsymbol{M_y}$, $\boldsymbol{M_z}$) as shown in Fig. 7. According to two dimension analysis, the expressions for the corresponding force and moment equilibrium in different configuration can be derived as follows:

$$\sum \vec{M} = \vec{M}_{ext} + \sum_{i=1}^{m}\left(\left(\vec{R}_i \times f_i\vec{n}_i\right) - \left(\vec{R}_i \times \mu f_i\vec{v}_i\right)\right) \tag{81}$$

$$\sum \vec{F} = \vec{F}_{ext} + \sum_{i=1}^{m}\left(f_i\vec{n}_i - \mu f_i\vec{v}_i\right) \tag{82}$$

where $\vec{n}_i$ and $\vec{v}_i$ are the unit normal and unit velocity vector, respectively, of the *i*th contact point between the peg and hole.

In three dimensional subspaces, the constraint expressions for sliding the peg into hole can be represented as surfaces. For symmetrical cylindrical parts, the limitation of *z* directional moment can be ignored. The no-jamming space can be shown in Fig. 8. Since many parts do not exhibit rotational symmetry, this analysis can also be applied to other dissymmetrical parts.

To sum up, in order to avoid jamming, we must guarantee the conditions of the appropriate force/torque proportion. Based on the relations of input forces and moments, proper assembly strategies can be taken.

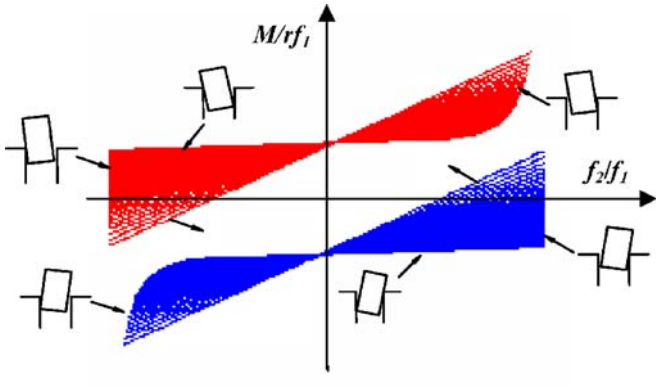

Fig. 6 The jamming diagram

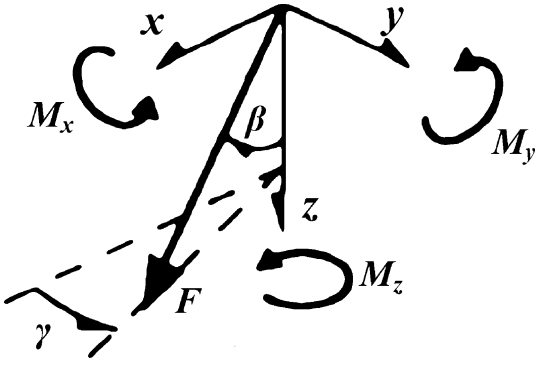

Fig. 7 Representation of applied force and moment

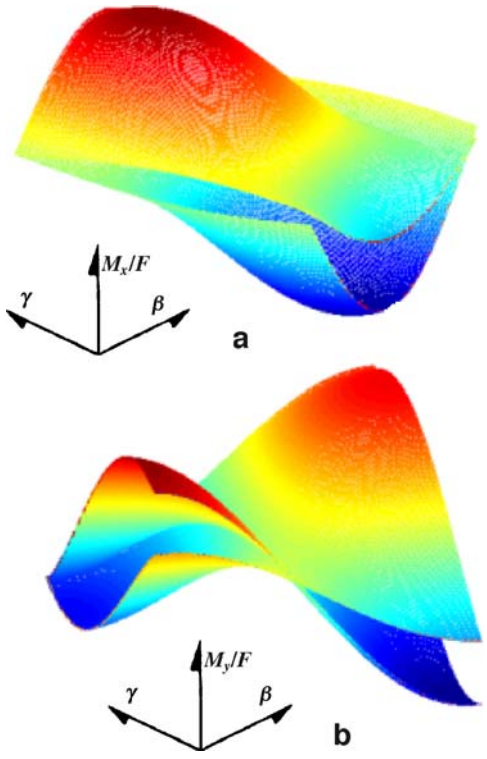

Fig. 8 Three dimension no–jamming space

4.2 Wedging analysis

Wedging is also a condition in which the peg appears stuck in the hole, but unlike jamming, the cause is static geometric condition rather than ill-proportioned applied forces and moments. Wedging can arise in such a system that there are two or more constraints. In fact, it is a phenomenon which occurs when the resultant forces at the constraints are linearly dependent and are inside the friction cone or at the edge of the friction cone. It cannot be avoided by increasing or reducing the input forces and moments. In peg-in-hole process, wedging may occur at two-point contact situation [12]. In wedging, the two contact forces $f_{A\varepsilon}$ and $f_{B\varepsilon}$ can point directly opposite to each other. When either of the contact forces is outside its friction cone, i.e., either of the contact points is outside the friction cone of the other point, this phenomena is not possible. Consider the relations of friction cones and contact points, point B is outside the friction cone of point A earlier than point A outside the point B′s. So, when the contact point B is outside the friction cone of point A, there is no wedging. Using geometrical constraints, we have

$$\mu = \tan\alpha \tag{81}$$

$$\frac{l}{d} = \tan\alpha_A \tag{82}$$

$$\frac{|y_{Bc}|}{D + \delta_A + \delta_B} = \tan\alpha_B \tag{83}$$

when $\theta > 0$, then $\alpha_A > \alpha_B$. So

$$\tan\alpha_A = \frac{l}{d} > \mu. \tag{84}$$

Substituting Eq. 24 to 84

$$\theta < \arcsin\left(\frac{D + \delta_B}{\sqrt{(\mu d)^2 + (d - \delta_A)^2}}\right) - \varphi = \theta_c \tag{85}$$

where $\varphi = a\tan\left(\frac{d - \delta_A}{\mu d}\right)$.

For small clearance ratio,

$$\theta < \mu c = \theta_c. \tag{86}$$

4.3 Strategies for assembly

For special assembly task, the geometric information, the characteristic of material, the directions of the input forces and moments, the time of motion, the initial and final velocities of the peg are generally given apriori. And the values are $r, R, l_c, l_i, l_f, m, J, \mu_s, \mu_k, E, \nu, f_1, t_i, t_f, \dot{l}_i, \dot{l}_f, \ddot{l}_i, \ddot{l}_f$, etc. The value of the insertion depth l and the direction of θ at any time can be measured by the robot controller or sensors after determining the position of the peg in the hole. When the peg is counterclockwise turned, the direction of tilt angle θ is positive and vice versa. The insertion depth and tilt angle are changeable with time. It is assumed that the insertion depth l is a certain function of insertion time, such as different kinds of polynomial functions or some nonlinear functions. Based on the above conditions, the insertion depth and tilt angle can be obtained at any time. If the contact state is one-point contact, which has two degrees of freedom, the tilt angle cannot be obtained by this way, but it is less than the tilt angle of the two-point contact state. In an assembly process, the insertion depth is increasing and the tilt angle is decreasing with time, moreover, the chance of jamming and wedging is gradually reduced. Since it is necessary for successful assembly to avoid jamming and wedging, strategies of no-jamming and no-wedging are concerned at first. The successful rate of assembly and the efficiency of assembly are also important for assembly operation.

Firstly, in order to avoid dynamic jamming under all possible geometrical situations, a proper applied forces/moments proportion must be set. When the peg contacts the hole with two points, the adjustment of applied forces and moments is based on the constraint inequalities Eqs. 75,

78, 79, and 80. When one-point contact occurs, the proportion of applied forces at the X direction and the Y direction must satisfy one-point no jamming conditions.

Secondly, consider wedging is a static geometrical phenomenon, which cannot be avoided by adjusting the proportional relations of applied forces and moments. According to the wedging analysis in Sect. 3.2, wedging may occur when the tilt angle satisfies the condition $\theta_0 \leq \theta \leq \theta_c$. where θ_0 is the max tilt angle when the peg initially inserts the hole and θ_c is the critical wedging angle. If $\theta < \theta_c$, there is no wedging. However, the tilt angle doesn't continuously change and it is not certain when states change in the assembly process. So the no-wedging condition can be obtained from inequality Eq. 84 and the insertion depth can be obtained from a certain time function.

Finally, sum up the no-jamming and no-wedging conditions, the active assembly strategy can be presented. At the initial assembly time, the one-point contact state isn't taken as the initial assembly state untill the inequality Eq. 84 is satisfied. As a result, the assembly operation can be successful through the adjustment of applied forces and moments.

5 Conclusion

Under traditional Hertz contact theory, the unilateral contact conditions, friction model, and elastic contact are analyzed in this paper. The elastic contact dynamical model of peg-in-hole is established based on compliant contact model and geometrical constraints. It is more accurate than traditional rigid dynamic models. Deformation can change the constraint space and geometrical states. The constraint Jacobian matrix can be obtained by deformation and geometrical constraint conditions. In the light of physical characteristic of the system and constraint Jacobian matrices, we can prove the system satisfied the principle of energy conservation. It proves that the model we have established is correct. Based on the dynamical model, the forces/moments and geometric conditions for jamming and wedging are analyzed and the no-jamming and no-wedging assembly strategies are taken accordingly. From the analysis for the insertion of a cylindrical peg into a hole, we can extend the method to some symmetrical or dissymmetrical parts assembly. The assembly strategies were implemented and tested. For the assembly task, a robot operating under force control was used.

References

1. Mason MT, Wang Y (1988) On the inconsistency of rigid-body frictional planar mechanics. IEEE Conf. Robotic and Automation, Philadelphia, pp 524−528
2. Wang Y, Mason MT (1987) Modeling impact dynamics for robotic operations. IEEE Int Conf Robot Autom 2:678−685
3. Rajan VT, Burridge R, Schwartz JT (1987) Dynamics of a rigid body in frictional contact with rigid walls. IEEE Int Conf Robot Autom 2:671−677
4. Sinha PR, Abel JM (1992) A contact stress model for multifingered grasps of rough objects. IEEE Trans Robot Automat 8(1):7−22
5. Mei FX, Liu GL (1987) Basis of analytical mechanics. Xi'an Jiaotong University Press, Xi'an, China
6. Pierre ED, Serge PY (1997) Stability of Frictional Contact in Constrained rigid-body dynamic. IEEE Trans Robot Automat 13(2):230−236
7. Austin D, McCarragher B (1997) Force control command synthesis for assembly using a discrete event framework. IEEE Int Conf Robot Autom, pp 933−938
8. Defozino TL, Seltver DS, Whitney DE (1984) Instrumented remote center compliance. Ind Rob, pp 238−248
9. Sturges RH, Laowattana S (1994) Passive assembly of non-axisymmetric rigid parts. IEEE/RSJ Int Conf on Intelligent Robots and System, pp 1218−1225
10. Asada H, Kakumoto Y (1988) The dynamic RCC hand for high-speed assembly. IEEE Int Conf Robot Autom, pp 120−125
11. Seyfferth W, Pferffer F (1992) Dynamics of assembly processes fwith a manipulator. IEEE/RSJ Int Conf on Int Robots and Systems, pp 1303−1310
12. Whitney DE (1982) Quasi-static assembly of compliantly supported rigid parts. J Dyn Syst, Measure Control 104(2):65−77
13. Villarreal A, Asada H (1991) A geometric representation of distributed compliance for the assembly of flexible parts. IEEE Conf Robot Autom, pp 2708−2715
14. Meitinger T, Pfeiffer F (1994) Automated assembly with compliant mating parts. IEEE Conf Robot Autom, 1462−1467